Hindawi Publishing Corporation
Journal of Nanomaterials
Volume 2013, Article ID 915461, 12 pages
http://dx.doi.org/10.1155/2013/915461

Research Article

Influences of Stacking Architectures of TiO_2 Nanoparticle Layers on Characteristics of Dye-Sensitized Solar Cells

Chih-Hung Tsai,[1] Yu-Tang Tsai,[2] Tsung-Wei Huang,[2] Sui-Ying Hsu,[2] Yan-Fang Chen,[2] Yuan-Hsuan Jhang,[2] Lun Hsieh,[2] Chung-Chih Wu,[2] and Yen-Shan Chen[3]

[1] *Department of Opto-Electronic Engineering, National Dong Hwa University, Hualien 97401, Taiwan*
[2] *Department of Electrical Engineering, Graduate Institute of Photonics and Optoelectronics, Graduate Institute of Electronics Engineering, and Innovative Photonics Advanced Research Center (i-PARC), National Taiwan University, Taipei 10617, Taiwan*
[3] *AU Optronics Corporation, Hsinchu 30078, Taiwan*

Correspondence should be addressed to Chih-Hung Tsai; cht@mail.ndhu.edu.tw and Chung-Chih Wu; chungwu@cc.ee.ntu.edu.tw

Received 3 January 2013; Revised 17 March 2013; Accepted 25 March 2013

Academic Editor: Marinella Striccoli

We investigated the influences of stacking architectures of the TiO_2 nanoparticle layers on characteristics and performances of DSSCs. TiO_2 nanoparticles of different sizes and compositions were characterized for their morphological and optical/scattering properties in thin films. They were used to construct different stacking architectures of the TiO_2 nanoparticle layers for use as working electrodes of DSSCs. Characteristics and performances of DSSCs were examined to establish correlation of the stacking architectures of TiO_2 nanoparticle layers with characteristics of DSSCs. The results suggest that the three-layer DSSC architecture, with sandwiching a 20 nm TiO_2 nanoparticle layer between a 37 nm TiO_2 nanoparticle layer and a hundred nm sized TiO_2 back scattering/reflection layer, is effective in enhancing DSSC efficiencies. The high-total-transmittance 37 nm TiO_2 nanoparticle layer with a larger haze can serve as an effective front scattering layer to scatter a portion of the incident light into larger oblique angles and therefore increase optical paths and absorption.

1. Introduction

Increasing energy demands and concerns about global warming have encouraged scientists to develop low-cost and easily accessible renewable energy sources in recent years. Dye-sensitized solar cells (DSSCs) offer the advantages of relatively high efficiencies, simple device structures, cost-effective manufacturing, and variety and flexibility in applications thus emerging as one of the most promising solar cell technologies [1–3]. A typical DSSC consists of a transparent conductive substrate, a porous thin-film photoelectrode composed of TiO_2 nanoparticles, dyes, an electrolyte, and a counter electrode [4]. In dye-sensitized solar cells (DSSCs), nanoporous thin-film electrodes composed of TiO_2 nanoparticles are a critical component [5–7], in terms of creating transport pathways for photo-generated electrons, providing high surface areas for the adsorption of dyes, and providing pores for the electrolyte solution to permeate [8–10]. In the early past, DSSCs used planar electrodes for dye adsorption and only dye molecules on the surface of the electrode could generate photocurrent, resulting in a power conversion efficiency of lower than 1% [11]. In 1991, Grätzel and his colleagues utilized porous TiO_2 nanoparticle thin-film electrodes to increase the surface areas for enhancing dye adsorption on the surface of the TiO_2 working electrode [12]. As such, the power conversion efficiency of the DSSCs was dramatically improved.

As the compositions and architectures of the TiO_2 electrodes is critical for preparation of efficient DSSCs [13–15], researchers had been engaged in investigating influences of the structures of TiO_2 electrodes on DSSC characteristics and performances [16–20]. In designing/optimizing the TiO_2 electrodes, usually there is a trade-off between the optical absorption/charge generation and the electrical/transport

properties (e.g., series resistance, charge recombination, open-circuit voltage, etc.) [21]. The optimized TiO_2 electrode thickness is thus typically less than the desired optical absorption length [22], and different compositions and architectures of the TiO_2 electrodes had been studied to enhance absorption and yet not degrading electrical/transport performances of DSSCs [23]. For instance, a typical TiO_2 photoelectrode of a DSSC includes a three-layer structure: a compact layer, a nanocrystalline layer, and a scattering layer. In some cases, the architecture for the TiO_2 nanoparticle electrode is composed of a layer of small nanoparticles (tens of nm) for larger surface areas and dye uptakes and a layer containing larger nanoparticles (hundreds of nm) as the back optical scattering/reflection layer for enhancing usage of the incident light [24–26]. In some other cases, TiO_2 electrodes composed of mixtures of small TiO_2 nanoparticles and significant portions of large TiO_2 particles are also used as the layer in front of the back scattering/reflection layer [27–29]. In such cases, even stronger scattering could be induced by the added large particles such that the originally weak absorption in some wavelength ranges (e.g., longer wavelengths) could be enhanced, yet with the risk of degrading originally efficient absorption in other wavelength ranges (e.g., shorter wavelengths) due to significant back scattering loss of the incident light [30]. It is therefore desired to have a TiO_2 nanoparticle electrode architecture that could provide some degree of optical (forward) scattering and yet also retain a high integrated transmittance to avoid back scattering loss of the incident light.

In this study, we investigated the influences of various stacking architectures of the TiO_2 nanoparticle layers on characteristics and performances of DSSCs. The TiO_2 nanoparticles of different sizes and compositions were characterized for their morphological and optical/scattering properties in thin films. Comprehensive characterization results of optical scattering properties (e.g., haze, total integrated transmittance, etc.) of various TiO_2 nanoparticles/compositions and their correlation with DSSC characteristics were studied. We found that under appropriate conditions/combinations, the front scattering can be beneficial to the DSSC efficiency. The 37 nm TiO_2 nanoparticle layer can provide a larger haze (i.e., stronger scattering) and yet still high total transmittance than the typical 20 nm TiO_2 nanoparticles. When using 37 nm TiO_2 nanoparticle as the front scattering layer for DSSCs, it can more effectively scatter a portion of the incident light into larger oblique angles and therefore increase optical paths and absorption, beneficial to DSSC efficiencies.

2. Experimental Details

2.1. Characterization of TiO_2 Nanoparticle Thin Films. Anatase TiO_2 nanoparticle pastes with four different particle sizes/compositions, T20 (20 nm), T37 (37 nm), D20 (20 nm particles mixed with a portion of large particles of 200–400 nm), and RSP (large particles of 200–400 nm) were purchased from Solaronix SA, Switzerland. The specifications of these TiO_2 nanoparticles are shown in Table 1. Their properties to be obtained from characterizations described below are also summarized in Table 1.

Scanning electron microscopy (SEM) was used to characterize the morphology of TiO_2 nanoparticle thin films and the TiO_2 nanoparticle sizes. Atomic force microscopy (AFM) was used to characterize the topography of TiO_2 nanoparticle thin films and their surface roughnesses. The thickness of the TiO_2 films was determined by a stylus-based surface profiler. A UV-Vis spectrophotometer equipped with an integrating sphere was used to characterize the transmittance and scattering properties of the 6 μm thick TiO_2 nanoparticle films. In this work, two types of transmittance were characterized: the total transmittance (T_{total}) and the direct transmittance (T_{direct}). T_{total} was measured by using a monochromatic light beam normally incident onto sample and then using an integrating sphere to collect transmitted light over all angles. On the other hand, T_{direct} was measured by using a monochromatic light beam normally incident onto the sample and then collecting transmitted light only in the normal direction (within a 5° collection angle). The haze values of TiO_2 films, which are defined as the ratio of the diffusively transmitted light against the total transmitted light [31], were then obtained by Haze $= (T_{\text{total}} - T_{\text{direct}})/T_{\text{total}}$ at some specific wavelength, which is useful indication of the optical scattering capability of a thin film.

2.2. DSSC Fabrication. DSSCs with different stacking architectures of TiO_2 nanoparticle layers were fabricated by using different TiO_2 nanoparticles. In fabrication of devices, the glass substrates coated with the transparent conductor fluorine-doped oxide (FTO) (Solaronix, TCO 22–15, with a sheet resistance of 15 $\Omega/\square$) were first cleaned in a detergent solution using an ultrasonic bath and then were rinsed with water and ethanol. The layered structure of the nanoporous TiO_2 working electrode using different TiO_2 nanoparticles was then coated onto FTO by the doctor-blade method. The nanoporous TiO_2 electrodes were then heated in an atmospheric oven first by gradually ramping the temperature from 150°C to 500°C and then at 500°C for 30 min. After cooling, the nanoporous TiO_2 electrodes were immersed into a dye solution at room temperature for 24 hours for dye adsorption. The dye solution was composed of 0.5 mM well-known ruthenium dye N719, [cis-di(thiocyanato)-N-N′-bis(2,2′-bipyridyl-4-carboxylic acid-4′-tetrabutyl-ammonium carboxylate) ruthenium (II)] [32], and 0.5 mM of chenodeoxycholic acid (CDCA, as a coadsorbent) in the acetonitrile/*tert*-butanol mixture (1 : 1) [33].

Counter electrodes of the DSSC were prepared by depositing 40 nm thick Pt films on other glass substrates by e-beam evaporation. The dye-adsorbed TiO_2 working electrode and a counter electrode were then assembled into a sealed DSSC with a sealant spacer (the thickness of the spacer is 25 μm) between the two electrode plates. A drop of the electrolyte solution (0.6 M 1-butyl-3-methylimidazolium iodide (BMII), 0.03 M I_2, 0.5 M 4-*tert*-butylpyridine, and 0.1 M guanidinium thiocyanate in a mixture of acetonitrile-valeronitrile (85 : 15, v/v)) was injected into the cell through a

Table 1: The properties of different TiO_2 nanoparticles and different TiO_2 nanoparticle films.

TiO_2 sample name	Particle size (nm)	Roughness (6 μm thick) (nm)	T_{total} (500 nm) (%)	Haze (500 nm) (%)
T20	20	8.69	86.6	7.2
T37	37	9.66	81.2	8.8
D20	20 + 200	32.26	52.4	92.2
RSP	200	77.52	16.3	99.7

drilled hole [34]. Finally, the hole was sealed. A mask with an aperture area of 0.125 cm^2 was covered on a testing cell before measurements. The total active area of the device is 0.125 cm^2.

2.3. DSSC Characterization. The photocurrent-voltage (I-V) characteristics of the DSSCs were measured under illumination of the simulated AM1.5 G solar light from a 300 W Xenon lamp solar simulator. The incident light intensity was calibrated as 100 mW/cm^2. Photocurrent-voltage curves were obtained by applying an external bias voltage to the cell and measuring the generated photocurrent. The current-voltage characteristics of DSSCs were used to extract the short-circuit current density (J_{SC}), open-circuit voltage (V_{OC}), fill factor (FF), and power conversion efficiency (η) of the DSSCs [35, 36].

The incident photon-to-current conversion efficiency (IPCE) spectra of the devices were measured by using a 75 W Xenon arc lamp as the light source coupled to a monochromator. The IPCE data were taken by illuminating monochromatic light on the solar cells (with the wavelength from 300 nm to 800 nm) and measuring the short-circuit current of the solar cells [37]. The IPCE measurement was performed with a lock-in amplifier, a low-speed chopper, and a bias light source under the full computer control.

In addition to the standard I-V and IPCE characterization of solar cells, in this study, the electrochemical impedance spectroscopy (EIS) was also used to analyze the internal impedance properties of DSSCs [38–40]. The electrochemical impedance spectroscopy of the cells was measured by using an impedance analyzer with a frequency range of 20 Hz to 1 MHz. In this study, during the impedance measurement, the cell was under the constant AM 1.5 G 100 mW/cm^2 illumination. The impedance of the cell (throughout the frequency range of 20 Hz to 1 MHz) was then measured by applying a bias at the open-circuit voltage V_{OC} of the cell (namely, under the condition of no DC electric current) and by using an AC amplitude of 10 mV.

3. Results and Discussions

3.1. Properties of TiO_2 Nanoparticle Thin Films. Figures 1 and 2 show the SEM and AFM images of the various TiO_2 nanoparticle films (6 μm thick). As shown in SEM images of Figure 1, T20 and T37 are composed of only small TiO_2 nanoparticles; D20 is composed of mostly small particles and yet also some large particles (>100 nm); RSP is composed of only large TiO_2 particles exceeding 100 nm. Also, the size of pores in the TiO_2 electrodes increases with the nanoparticles' size. With the size of larger particles in D20 and RSP being similar to the optical wavelengths, one may expect strong scattering effects from these samples, compared to T20 and T37. Topographical characteristics examined by AFM for these samples (Figure 2) are similar to/consistent with those observed by SEM. Yet the surface roughness can now be quantitatively determined from the AFM results. T20 and T37 films show smaller surface roughnesses of 8.69 and 9.66 nm, respectively, while D20 and RSP containing large particles show significantly greater surface roughnesses of 32.26 and 77.52 nm, respectively. The particle sizes and surface roughnesses of all samples are summarized in Table 1.

Figure 3 shows the total transmittance (T_{total}) and the direct transmittance (T_{direct}) spectra of the various TiO_2 nanoparticle films (6 μm thick). T_{total} and haze (calculated from T_{total} and T_{direct} spectra) of various TiO_2 nanoparticle films at the wavelength of 500 nm are also summarized in Table 1. As can be seen in Figure 3 and Table 1, increasing the nanoparticle size from 20 nm (T20) to 37 nm (T37) raises the haze value from 7.2% to 8.8%. T_{total} also drops (from 86.6% to 81.2%) but still remains a rather high value. Furthermore, the occurrence of larger particles (~200 nm, D20 and RSP films) largely raises haze values and thus the optical scattering capability. With mixing a small portion of large nanoparticles in the D20 film, the haze at 500 nm rises sharply to >90% and T_{total} drops to 52.4%. In the most dramatic case of the RSP film containing only large particles, the normal-direction transmittance T_{direct} is almost completely blocked, resulting in a small T_{total} of only 16.3%. A low T_{total} implies that most of the incident light cannot transmit through the film (either directly or by scattering) but is scattered backward/reflected instead. Due to low T_{total} of D20 and RSP films (strong back scattering/reflection), they are not suitable for use as the major active absorption layer in DSSC. In this work, we tested them as the optical scattering layer in some device architectures.

3.2. Characteristics of DSSCs with Varied Stacking Architectures of TiO_2 Nanoparticle Films. The various TiO_2 nanoparticle thin films were then subjected to DSSC studies. Figure 4 shows the schematic diagrams of various TiO_2 nanoparticle thin films. The influences of the various stacking architectures of TiO_2 nanoparticle thin films on the photovoltaic characteristics of the DSSCs were investigated.

We first examined the effects of the TiO_2 nanoparticle film thickness on DSSC characteristics, using single-layer T20 nanoparticle (particle size: 20 nm) thin-film electrodes having thicknesses of 8 μm, 12 μm, and 16 μm (Figures 4(a), 4(b), and 4(c)). Figure 5 shows the photocurrent density-voltage (J-V) characteristics and IPCE spectra of these

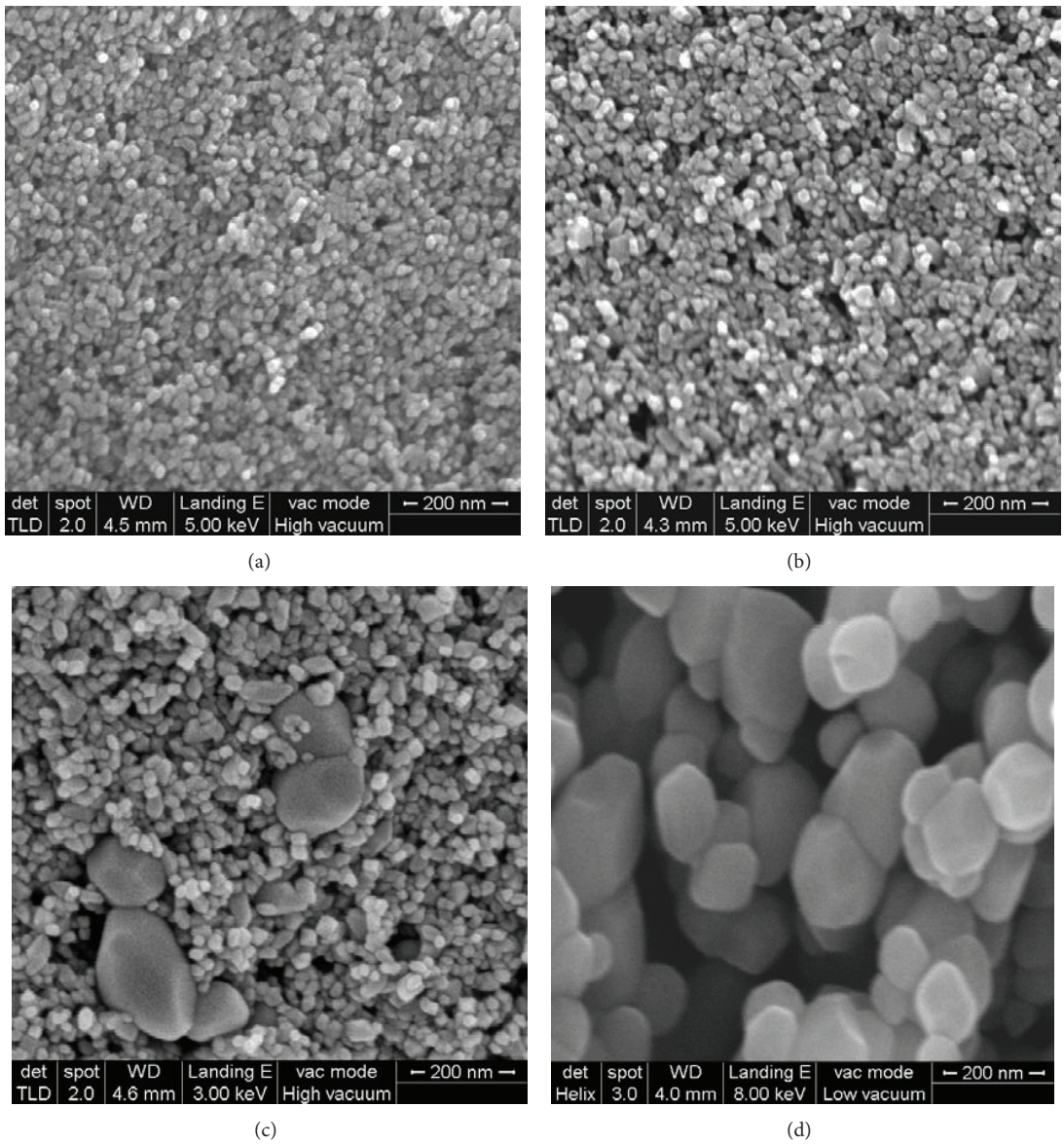

Figure 1: SEM images of the various TiO_2 nanoparticle films (6 μm thick): (a) T20, (b) T37, (c) D20, and (d) RSP.

DSSCs. Corresponding photovoltaic characteristics, short-circuit current J_{SC}, open-circuit voltage V_{OC}, fill factor FF, and power conversion efficiency are also summarized in Table 2. Results show that the IPCE and J_{SC} increase with the TiO_2 thickness, mainly because of enhanced absorption with thicker dye-loaded films. On the other hand, V_{OC} decreases with the TiO_2 thickness, suggesting some loss mechanisms of photogenerated carriers, such as electron recombination, in thicker films. T20 nanoparticle thin-film electrode having thickness of 16 μm gave higher current than 12 μm. T20 nanoparticle thin-film electrode having thickness of 16 μm gave lower efficiency than the 12 μm sample mainly due to the lower V_{OC}. Because of trade-offs between these competing mechanisms, the DSSC performances are optimized when the TiO_2 electrode has a thickness of about 12 μm, although it is not optimized for the strongest absorption. In all subsequent DSSC experiments, a total thickness of 12 μm was adopted for the TiO_2 absorption layer of DSSCs.

We then examined DSSCs containing a 12 μm thick T20 or T37 TiO_2 nanoparticle film, either with or without coating an extra 4-μm-thick RSP layer on top as the back scattering layer, yielding four combinations (T20, T20+RSP, T37, and T37+RSP) (Figures 4(b), 4(d), 4(e), and 4(f)). Figure 6 shows the *J-V* characteristics and the IPCE spectra for the T20 and the T20+RSP DSSCs, while Figure 7 shows the *J-V* characteristics and the IPCE spectra for the T37 and the T37+RSP DSSCs. Corresponding photovoltaic characteristics are also summarized in Table 2. For both T20 and T37 cases, devices with an additional back scattering/reflecting layer of 4 μm thick RSP nanoparticles exhibit significantly enhanced J_{SC} and power conversion efficiency (Figures 6(a) and 7(a), Table 2). The enhanced IPCE spectra with the

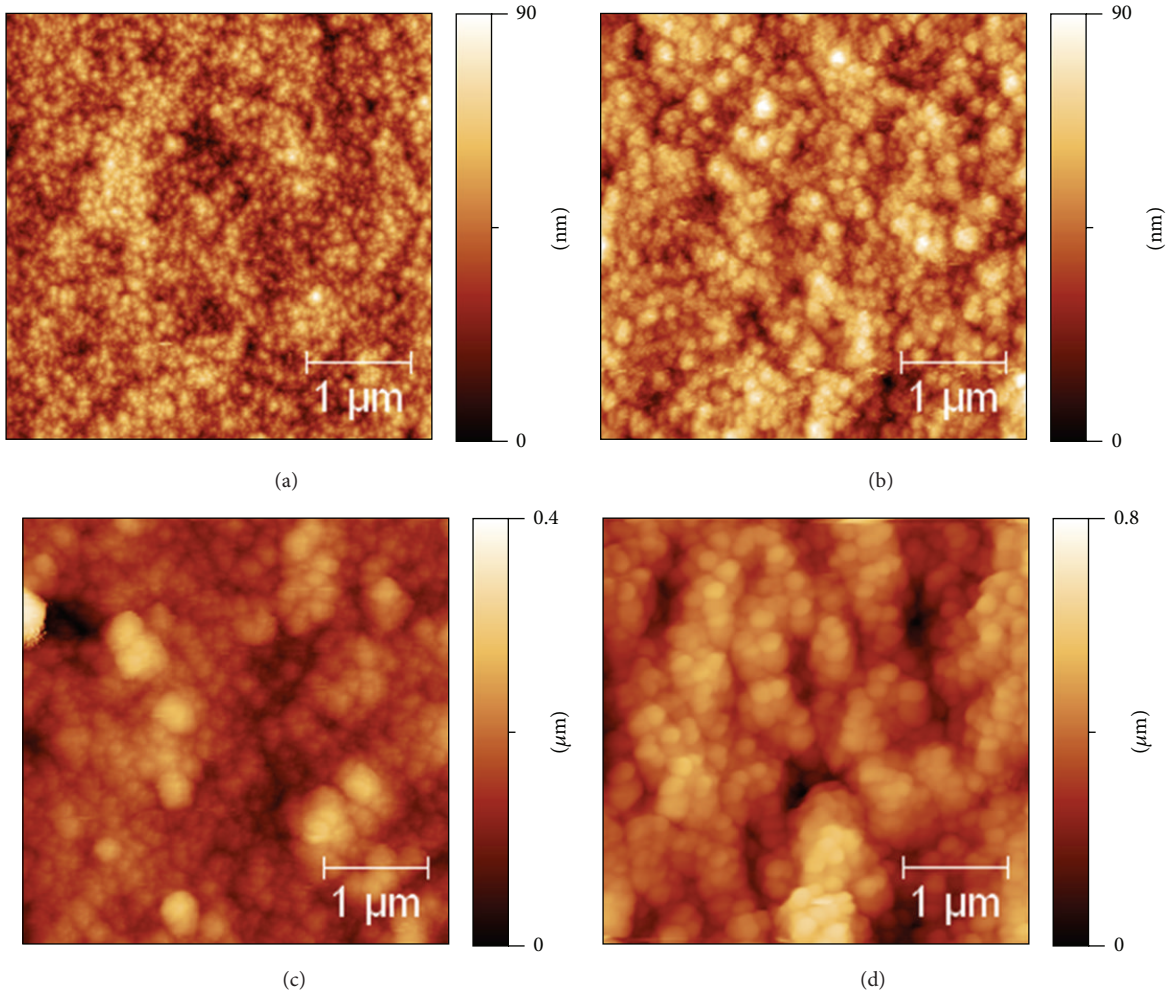

Figure 2: AFM images of the various TiO_2 nanoparticle films (6 μm thick): (a) T20, (b) T37, (c) D20, and (d) RSP.

Table 2: Photovoltaic characteristics of DSSCs with various stacking architectures of different TiO_2 nanoparticle layers.

TiO_2 electrode	Peak IPCE (%)	J_{SC} (mA/cm^2)	V_{OC} (V)	FF	Efficiency (%)
T20 (8 μm)	60.02	10.28	0.79	0.68	5.48
T20 (12 μm)	71.37	11.92	0.75	0.71	6.32
T20 (16 μm)	74.32	12.71	0.70	0.67	6.01
T20 (12 μm) + RSP (4 μm)	80.75	14.85	0.77	0.71	8.11
T37 (12 μm)	71.05	11.70	0.77	0.67	6.07
T37 (12 μm) + RSP (4 μm)	79.41	14.50	0.76	0.69	7.59
T20 (6 μm) + T37 (6 μm) + RSP (4 μm)	80.12	14.81	0.75	0.69	7.65
T37 (6 μm) + T20 (6 μm) + RSP (4 μm)	86.54	15.72	0.77	0.70	8.47
D20 (6 μm) + T20 (6 μm) + RSP (4 μm)	68.82	13.06	0.77	0.68	6.83

addition of the RSP back scattering/reflecting layer (Figures 6(b) and 7(b)) indicate that the enhanced J_{SC} and power conversion efficiency are due to more efficient absorption and use of the incident light with the optical back scattering. Among the T20 and T37 devices, the T20+RSP device shows higher conversion efficiency (8.11%) than the T37+RSP device (7.59%), perhaps due to larger dye uptakes with smaller nanoparticles.

Since the T37 nanoparticle layer exhibits stronger optical scattering than the T20 nanoparticle layer (haze in Table 1, 8.8% versus 7.2%) and yet still retains a high total transmittance, it may be used as the front scattering layer of a

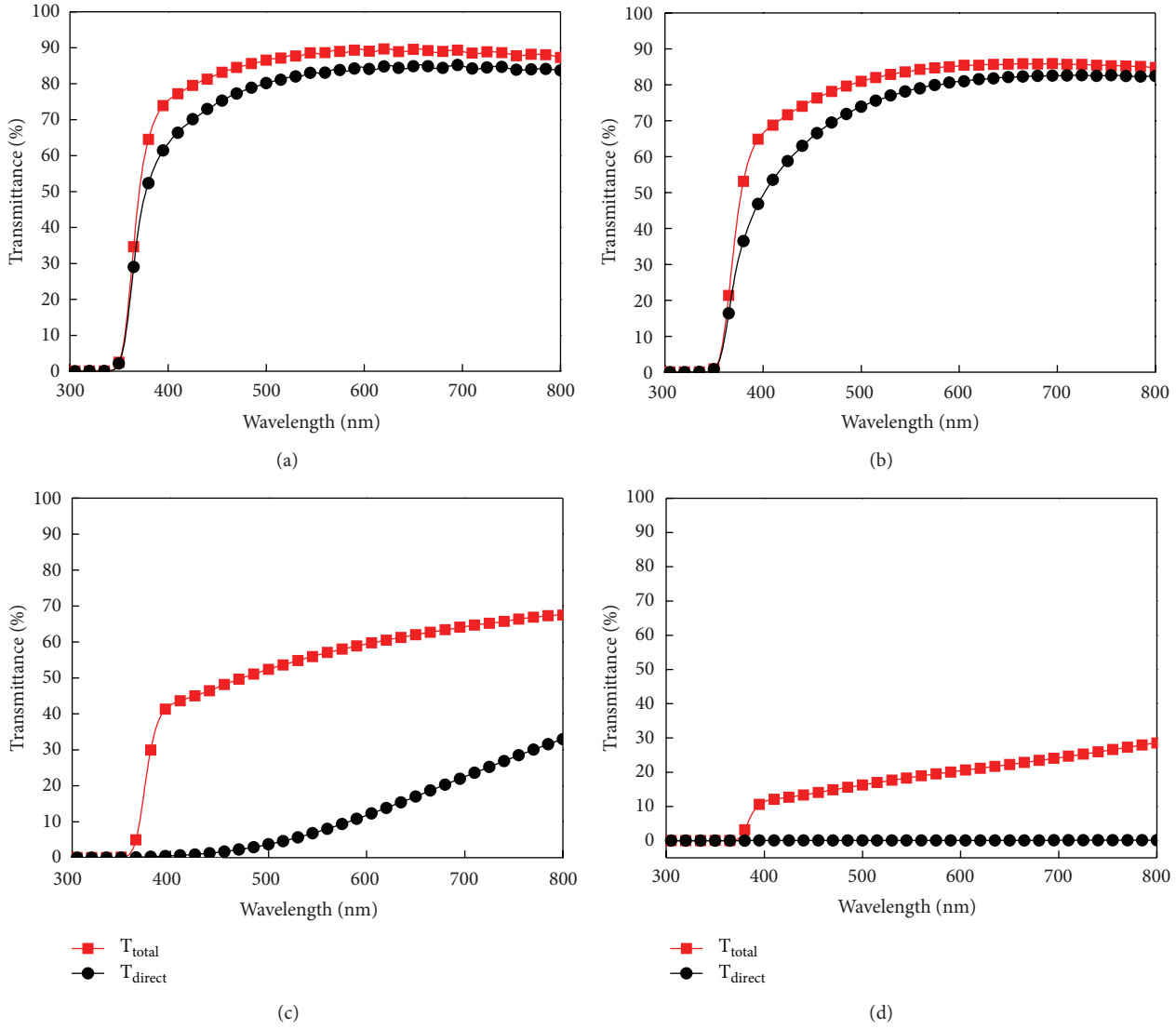

FIGURE 3: The total transmittance (T_{total}) and the direct transmittance (T_{direct}) spectra of the various TiO_2 nanoparticle films (6 μm thick): (a) T20, (b) T37, (c) D20, and (d) RSP.

DSSC to further boost efficiency. We thus further constructed the three-layer DSSC architecture by sandwiching a 6 μm T20 layer between a 6 μm T37 front scattering layer and a 4 μm RSP back scattering layer (Figure 4(g)). Figure 8 shows the J-V characteristics and the IPCE spectrum of the T37+T20+RSP DSSC, with its photovoltaic characteristics being summarized in Table 2. It is seen that with the T37 layer in front of the T20 layer, IPCE is increased from 80.75% of the T20+RSP two-layer architecture to 86.54% of the T37+T20+RSP three-layer architecture, leading to enhancement of J_{SC} from 14.85 mA/cm^2 to 15.72 mA/cm^2 and enhancement of conversion efficiency from 8.11% to 8.47%. For comparison, we also constructed two three-layer DSSCs D20+T20+RSP (Figure 4(h)) and T20+T37+RSP (Figure 4(i)). The D20 layer has much stronger optical scattering capability than the T37 layer (but also much lower total transmittance). The J-V characteristics and the IPCE spectrum of the D20+T20+RSP and T20+T37+RSP DSSCs are also shown in Figure 8, while their photovoltaic characteristics are summarized in Table 2. Compared to the T37+T20+RSP DSSC, the J_{SC}, IPCE, and conversion efficiency of the D20+T20+RSP and T20+T37+RSP three-layer devices all decrease. These results clearly indicate that the high-total-transmittance T37 layer with a larger haze can serve as an effective front scattering layer to scatter portion of the incident light into larger oblique angles and therefore increase optical paths and absorption.

3.3. Electrochemical Impedance Spectroscopy of Devices. The effects of stacking architectures of TiO_2 nanoparticle layers on characteristics of DSSCs were further investigated by electrochemical impedance spectroscopy (EIS). EIS is a useful tool for characterizing interfacial charge-transfer processes in DSSCs, such as the charge recombination at the

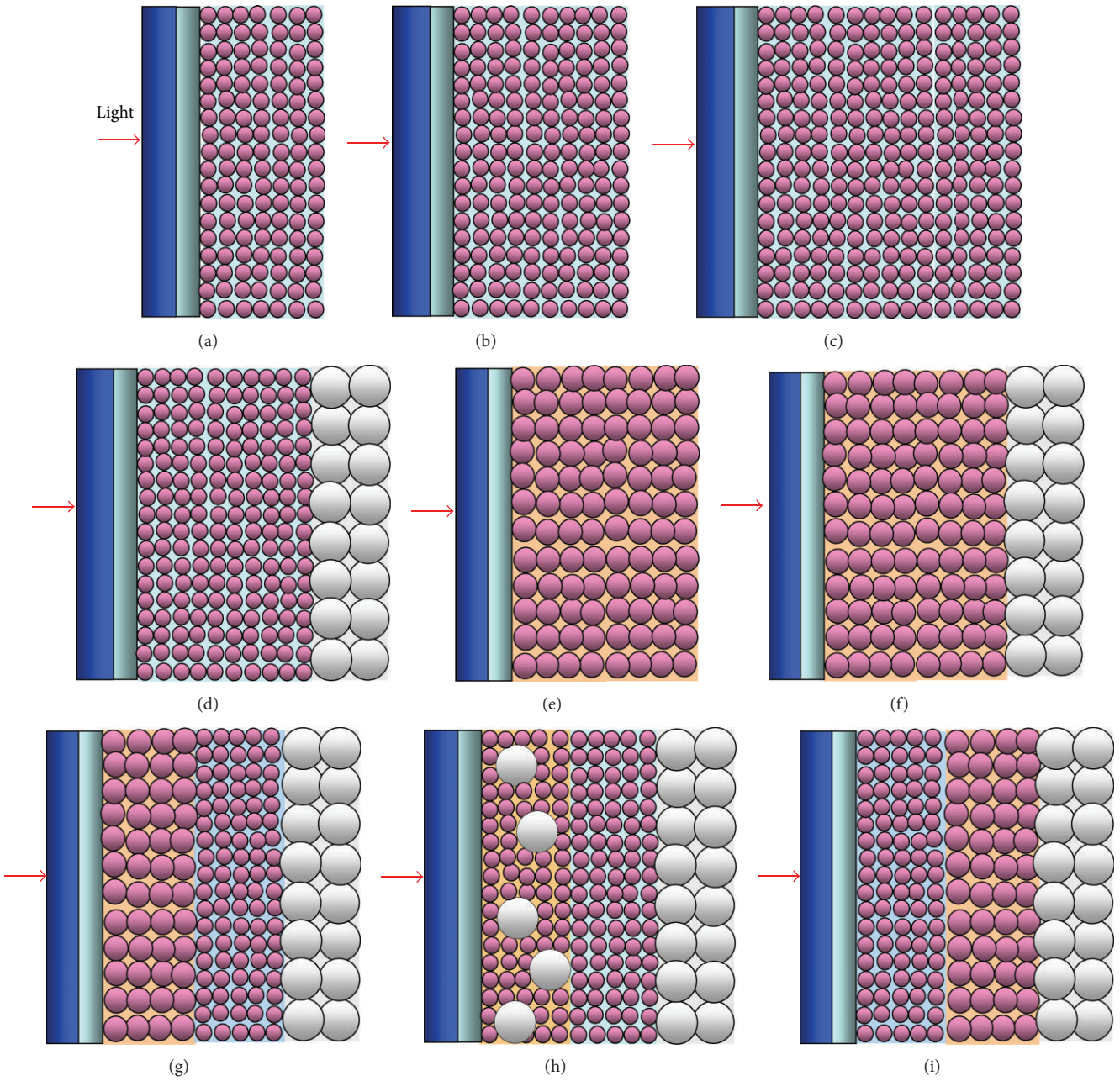

FIGURE 4: Schematic diagrams of the stacking architectures of TiO_2 nanoparticle layers: (a) T20 (8 μm), (b) T20 (12 μm), (c) T20 (16 μm), (d) T20 (12 μm)+RSP (4 μm), (e) T37 (12 μm), (f) T37 (12 μm)+RSP (4 μm), (g) T37 (6 μm)+T20 (6 μm)+RSP (4 μm), (h) D20 (6 μm)+T20 (6μm)+RSP (4 μm), and (i) T20 (6 μm)+T37 (6 μm)+RSP (4 μm).

TiO_2/dye/electrolyte interface, electron transport in the TiO_2 electrode, electron transfer at the counter electrode, and ion transport in the electrolyte [41, 42]. In this study, EIS was conducted by subjecting the cell to the constant AM 1.5G 100 mW/cm^2 illumination and to the bias at the open-circuit voltage V_{OC} of the cell (namely, the condition of no DC current).

Figure 9 shows the EIS Nyquist plots (i.e., minus the imaginary part of the impedance-Z'' versus the real part of the impedance Z' when sweeping the frequency) for the T20 single-layer device, the T20+RSP two-layer device, and the T37+T20+RSP three-layer device. In the frequency range investigated (20 Hz to 1 MHz), a larger semicircle occurs in the lower frequency range (~20 Hz to 1 kHz) and a smaller semicircle occurs in the higher frequency range. The larger semicircles in the lower frequency range (~20 Hz to 1 kHz) are not complete due to the limited frequency range of our instrument (the lowest frequency is not low enough). With the bias illumination and voltage applied, the larger semicircle at lower frequencies mainly corresponds to the charge-transfer

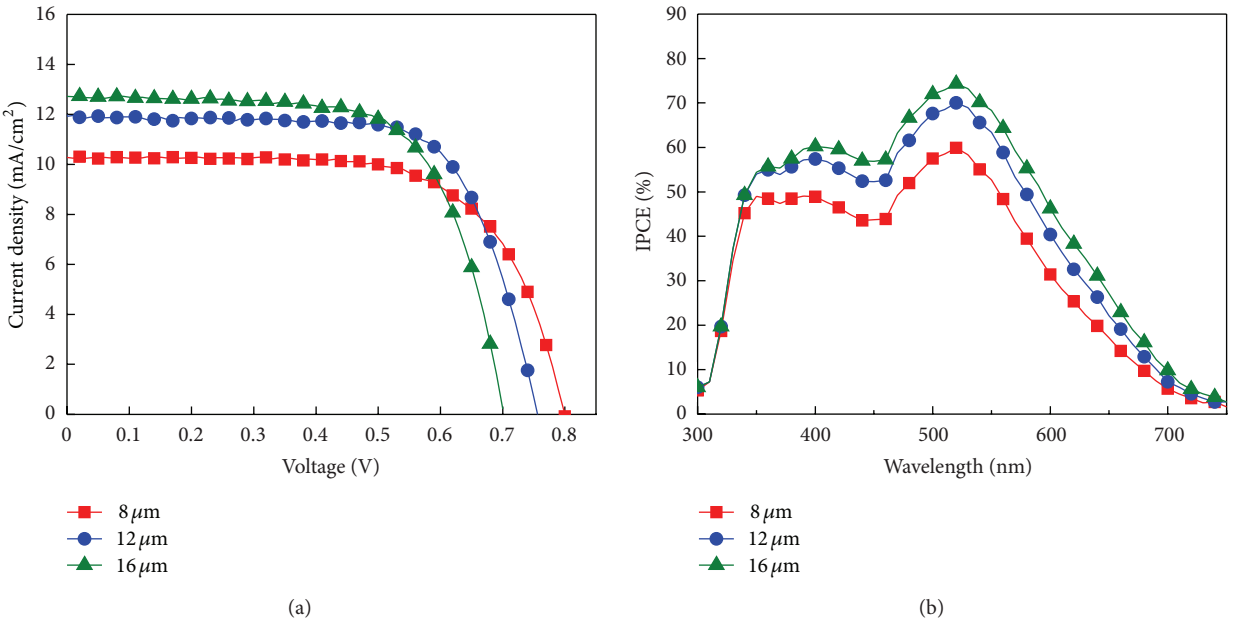

FIGURE 5: (a) Photocurrent density-voltage (J-V) characteristics and (b) IPCE spectra of DSSCs using single-layer T20 nanoparticle thin-film electrodes having thicknesses of 8 μm, 12 μm, and 16 μm.

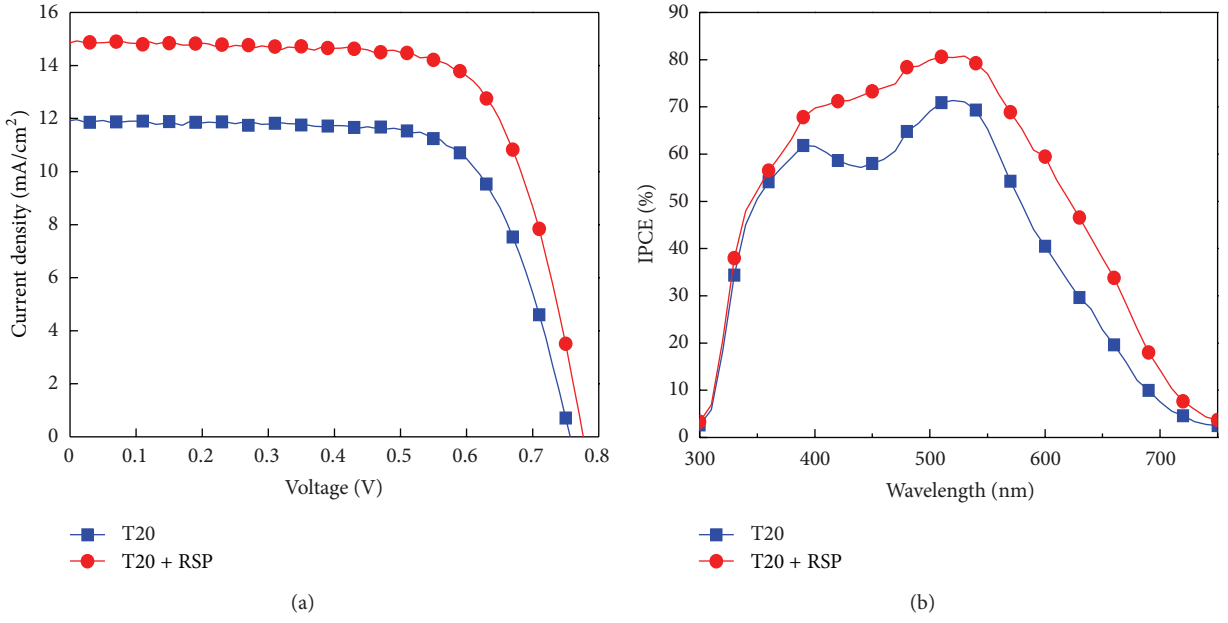

FIGURE 6: Comparison of (a) photocurrent density-voltage (J-V) characteristics and (b) IPCE spectra of DSSCs using the single-layer T20 nanoparticle electrode and the T20+RSP two-layer nanoparticle electrode.

processes at the TiO_2/dye/electrolyte interface [43], while the smaller semicircle at higher frequencies mainly corresponds to the charge-transfer processes at the Pt/electrolyte interface [44]. The intercept on the horizontal axis (Z') represents the series resistance of the device [45], which is associated with the sheet resistance of the FTO. Consistently, the three devices show same series resistances since same FTO substrates were used.

To extract quantitative impedance characteristics of the DSSCs, the measured impedance characteristics in Figure 9 were reproduced using the equivalent circuit shown in Figure 10 [46]. The series resistance R_S is associated with

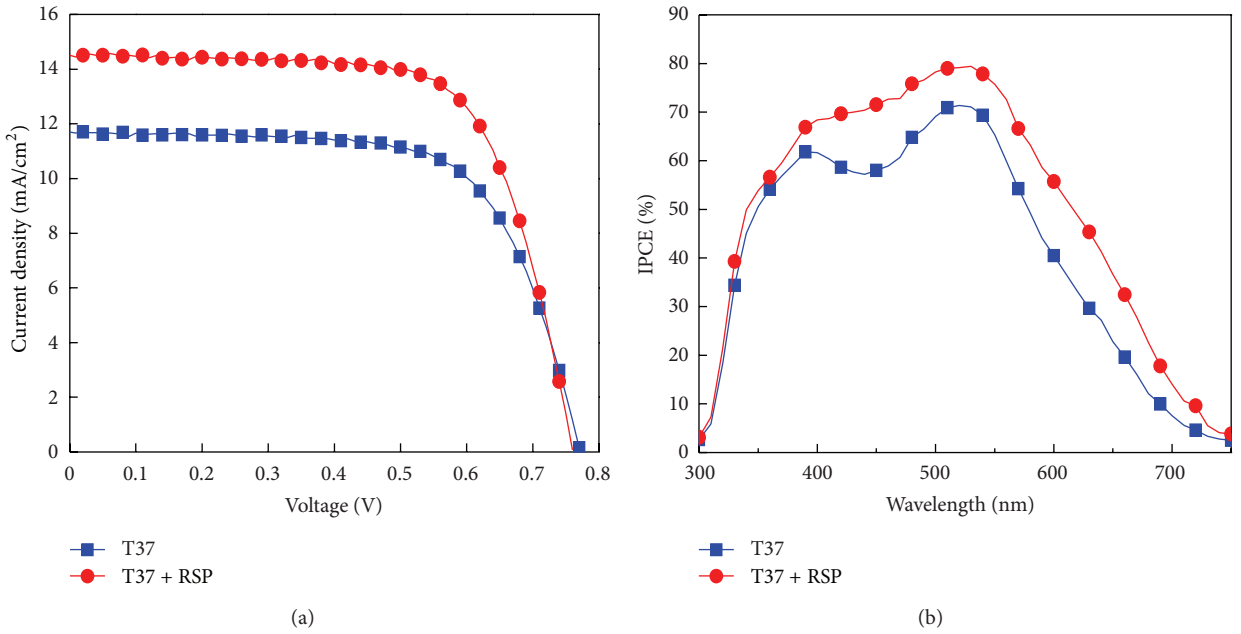

FIGURE 7: Comparison of (a) photocurrent density-voltage (J-V) characteristics and (b) IPCE spectra of DSSCs using the single-layer T37 nanoparticle electrode and the T37+RSP two-layer nanoparticle electrode.

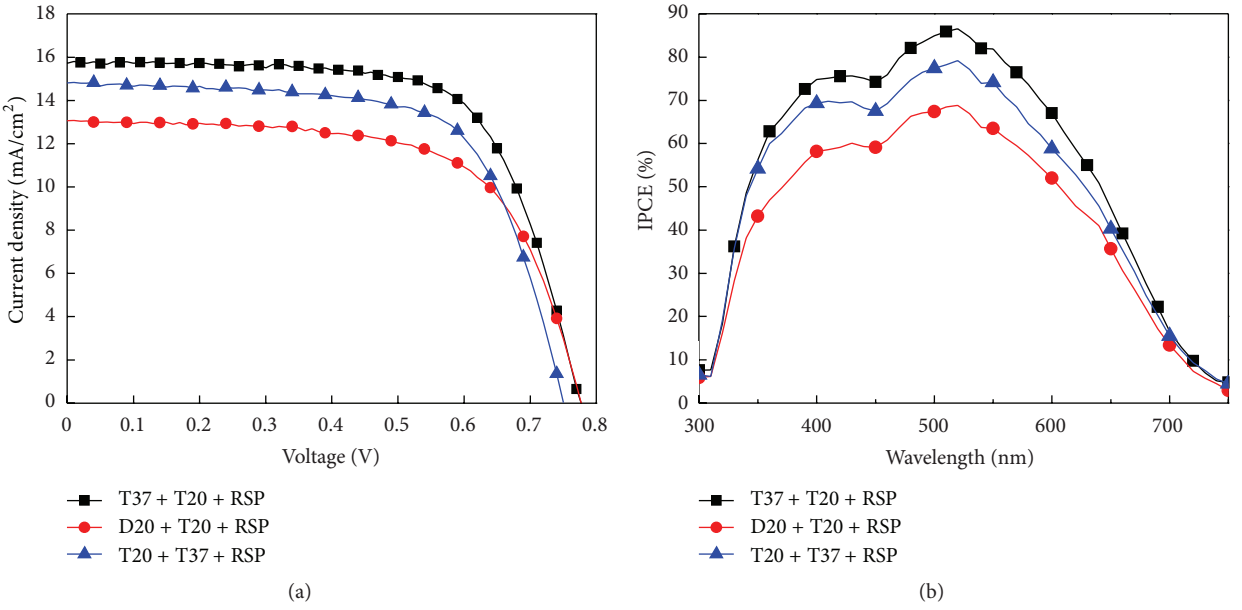

FIGURE 8: (a) Photocurrent density-voltage (J-V) characteristics and (b) IPCE spectra of DSSCs using the T37+T20+RSP, D20+T20+RSP, and T20+T37+RSP three-layer nanoparticle electrodes.

the contribution from the FTO and counter electrodes. The resistance R_{Pt} in parallel with the constant phase element CPE_{pt} is associated with the impedance at the Pt/electrolyte interface [47]. The impedance of a constant phase element (CPE) has the general form of $Z(\omega) = Q(j\omega)^{-\alpha}$, where ω is the angular frequency, Q the CPE parameter, and α the CPE exponent. Q is a constant parameter, and the parameter α can assume values between 0 and 1 [48]. The parameter α describes the degree of the capacitive character; when $\alpha = 1$, the CPE is like a regular capacitance. The CPE distributed element is introduced to account for dispersive characteristics of the interfacial capacitance, which are induced by spatial inhomogeneities (e.g., roughness) of the Pt/electrolyte interface [49]. The resistance R_{ct} in parallel with the capacitance C_μ is associated with the impedance at the TiO_2/dye/electrolyte interface [50], in which R_{ct} and C_μ represent the charge-transfer resistance and the chemical capacitance at the TiO_2/dye/electrolyte interface, respectively.

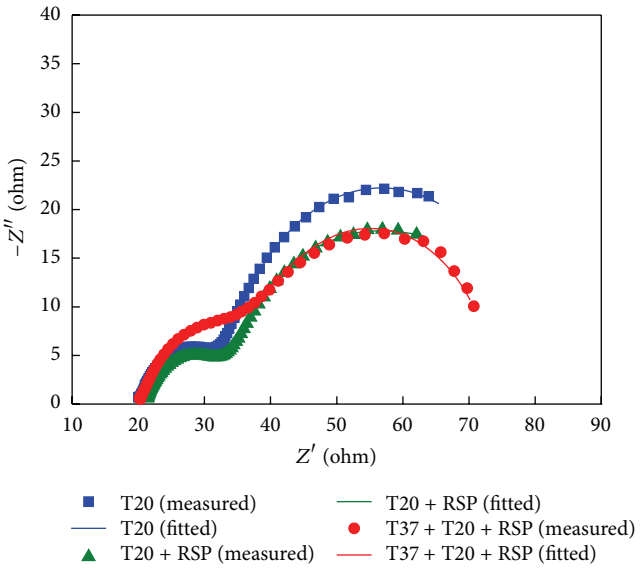

FIGURE 9: Measured and calculated EIS Nyquist plots for the T20 single-layer device, the T20+RSP two-layer device, and the T37+T20+RSP three-layer device.

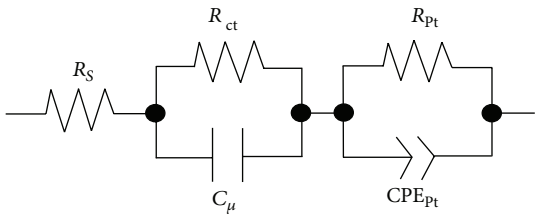

FIGURE 10: Equivalent circuit used to reproduce measured Nyquist plots shown in Figure 9.

TABLE 3: The parameters used to fit the EIS Nyquist plots of the three devices in Figure 9.

TiO_2 electrode	T20	T20 + RSP	T37 + T20 + RSP
R_S (ohm)	19.87	21.02	20.14
R_{Pt} (ohm)	15.19	14.97	15.12
CPE_{Pt} (Q/α)	$1.66 \times 10^4/0.73$	$1.50 \times 10^4/0.72$	$1.61 \times 10^4/0.78$
R_{Ct} (ohm)	43.32	34.35	32.24
C_μ (F)	1.15×10^{-4}	1.39×10^{-4}	7.63×10^{-5}

In the equivalent circuit shown in Figure 10, the electron transport (diffusion) resistance in the TiO_2 nanoparticles is neglected due to biasing at V_{OC}. Also, the impedance of the electrolyte is not considered since its effects occur at much lower frequencies (i.e., out of the frequency range investigated in this study). As shown in Figure 9, by carefully adjusting the device parameters, each curve in the Nyquist plot (each associated with a device architecture) can be well reproduced using the equivalent circuit of Figure 10. The parameters used to fit the curves for different devices are shown in Table 3.

In Table 3, one sees that the properties associated with the series resistance and the Pt/electrolyte interface remain similar for the three different devices, as one would expect. The extracted charge-transfer resistance R_{ct} (for the TiO_2/dye/electrolyte interface) of the T20 single-layer device, the T20+RSP two-layer device, and the T37+T20+RSP three-layer device is 43.32 Ω, 34.35 Ω, and 32.24 Ω, respectively. The decrease of R_{ct} with the increase of the DSSC efficiency indicates that electron generation and transfer at the TiO_2/dye/electrolyte interface are enhanced with more efficient absorption and use of the incident photons [51], consistent with photovoltaic characteristics of devices. Among these three devices, the T37+T20+RSP device gives the smallest R_{ct}, which corresponds to the optimal light harvesting and electron generation due to the high-total-transmittance front scattering layer (T37) and the effective back scattering layer (RSP). The higher C_μ of the T20+RSP cell than the single-layer T20 cell is also associated with more efficient carrier generation, while the lower C_μ of the T37+T20+RSP cell (versus the T20 cell and the T20+RSP cell) is perhaps associated with reduced surface areas of TiO_2 nanoparticle layers (when incorporating larger T37 nanoparticles in absorption layers) [52]. In general, the EIS results are in good agreement with results of the short-circuit currents and the overall power conversion efficiencies of the DSSCs.

4. Conclusions

In conclusion, we investigated the influences of stacking architectures of the TiO_2 nanoparticle layers on characteristics and performances of DSSCs. TiO_2 nanoparticles of different sizes and compositions were characterized for their morphological and optical/scattering properties in thin films. They were used to construct different stacking architectures of the TiO_2 nanoparticle layers for use as working electrodes of DSSCs. Characteristics and performances of DSSCs were examined to establish correlation of the stacking architectures of TiO_2 nanoparticle layers with characteristics of DSSCs. The results suggest that the three-layer DSSC architecture, with sandwiching a 20 nm TiO_2 nanoparticle layer between a 37 nm TiO_2 nanoparticle layer and a hundred nm sized TiO_2 back scattering/reflection layer, is effective in enhancing DSSC efficiencies. The high-total-transmittance 37 nm TiO_2 nanoparticle layer with a larger haze can serve as an effective front scattering layer to scatter a portion of the incident light into larger oblique angles and therefore increase optical paths and absorption.

Acknowledgments

The authors gratefully acknowledge the financial support from AU Optronics Corporation and the National Science Council of Taiwan.

References

[1] M. K. Nazeeruddin, R. Humphry-Baker, P. Liska, and M. Grätzel, "Investigation of sensitizer adsorption and the influence of protons on current and voltage of a dye-sensitized nanocrystalline TiO_2 solar cell," *The Journal of Physical Chemistry B*, vol. 107, no. 34, pp. 8981–8987, 2003.

[2] C. Y. Chen, M. Wang, J. Y. Li et al., "Highly efficient light-harvesting ruthenium sensitizer for thin-film dye-sensitized solar cells," *ACS Nano*, vol. 3, no. 10, pp. 3103–3109, 2009.

[3] J. Jiu, S. Isoda, F. Wang, and M. Adachi, "Dye-sensitized solar cells based on a single-crystalline TiO_2 nanorod film," *The Journal of Physical Chemistry B*, vol. 110, no. 5, pp. 2087–2092, 2006.

[4] A. Hagfeldt and M. Grätzel, "Molecular photovoltaics," *Accounts of Chemical Research*, vol. 33, no. 5, pp. 269–277, 2000.

[5] A. Hagfeld and M. Grätzel, "Light-induced redox reactions in nanocrystalline systems," *Chemical Reviews*, vol. 95, no. 1, pp. 49–68, 1995.

[6] M. Grätzel, "Photoelectrochemical cells," *Nature*, vol. 414, no. 6861, pp. 338–344, 2001.

[7] Y. Chiba, A. Islam, Y. Watanabe, R. Komiya, N. Koide, and L. Han, "Dye-sensitized solar cells with conversion efficiency of 11.1%," *Japanese Journal of Applied Physics*, vol. 45, no. 24–28, pp. L638–L640, 2006.

[8] M. K. Nazeeruddin, S. M. Zakeeruddin, R. Humphry-Baker et al., "Acid-base equilibria of (2,2′-bipyridyl-4,4′-dicarboxylic acid)ruthenium(II) complexes and the effect of protonation on charge-transfer sensitization of nanocrystalline titania," *Inorganic Chemistry*, vol. 38, no. 26, pp. 6298–6305, 1999.

[9] T. Bessho, S. M. Zakeeruddin, C. Y. Yeh, E. W. G. Diau, and M. Grätzel, "Highly efficient mesoscopic dye-sensitized solar cells based on donor-acceptor-substituted porphyrins," *Angewandte Chemie International Edition*, vol. 49, no. 37, pp. 6646–6649, 2010.

[10] Q. Wang, S. Ito, M. Grätzel et al., "Characteristics of high efficiency dye-sensitized solar cells," *The Journal of Physical Chemistry B*, vol. 110, no. 50, pp. 25210–25221, 2006.

[11] R. Memming and H. Tributsch, "Electrochemical investigations on the spectral sensitization of gallium phosphide electrodes," *The Journal of Physical Chemistry*, vol. 75, no. 4, pp. 562–570, 1971.

[12] B. O'Regan and M. Grätzel, "A low-cost, high-efficiency solar cell based on dye-sensitized colloidal TiO_2 films," *Nature*, vol. 353, no. 6346, pp. 737–740, 1991.

[13] G. S. Kim, H. K. Seo, V. P. Godble, Y. S. Kim, O. B. Yang, and H. S. Shin, "Electrophoretic deposition of titanate nanotubes from commercial titania nanoparticles: application to dye-sensitized solar cells," *Electrochemistry Communications*, vol. 8, no. 6, pp. 961–966, 2006.

[14] P. Wang, S. M. Zakeeruddin, J. E. Moser et al., "Stable new sensitizer with improved light harvesting for nanocrystalline dye-sensitized solar cells," *Advanced Materials*, vol. 16, no. 20, pp. 1806–1811, 2004.

[15] S. Uchida, R. Chiba, M. Tomiha, N. Masaki, and M. Shirai, "Application of titania nanotubes to a dye-sensitized solar cell," *Electrochemistry*, vol. 70, no. 6, pp. 418–420, 2002.

[16] M. K. Nazeeruddin, P. Péchy, and M. Grätzel, "Efficient panchromatic sensitization of nanocrystalline TiO_2 films by a black dye based on a trithiocyanato-ruthenium complex," *Chemical Communications*, no. 18, pp. 1705–1706, 1997.

[17] H. Y. Yang, Y. S. Yen, Y. C. Hsu, H. H. Chou, and J. T. Lin, "Organic dyes incorporating the dithieno[3,2-b:2′,3′-d]thiophene moiety for efficient dye-sensitized solar cells," *Organic Letters*, vol. 12, no. 1, pp. 16–19, 2010.

[18] R. W. Siegel, S. Ramasamy, H. Hahn, Z. Li, T. Lu, and R. Gronsky, "Synthesis, characterization, and properties of nanophase TiO_2," *Journal of Materials Research*, vol. 3, no. 6, pp. 1367–1372, 1988.

[19] J. W. Shiu, C. M. Lan, Y. C. Chang, H. P. Wu, W. K. Huang, and E. W. G. Diau, "Size-controlled anatase titania single crystals with octahedron-like morphology for dye-sensitized solar cells," *ACS Nano*, vol. 6, pp. 10862–10873, 2012.

[20] J. Song, H. B. Yang, X. Wang et al., "Improved utilization of photogenerated charge using fluorine-doped TiO_2 hollow spheres scattering layer in dye-sensitized solar cells," *ACS Applied Materials & Interfaces*, vol. 4, pp. 3712–3717, 2012.

[21] T. Yamaguchi, N. Tobe, D. Matsumoto, and H. Arakawa, "Highly efficient plastic substrate dye-sensitized solar cells using a compression method for preparation of TiO_2 photoelectrodes," *Chemical Communications*, no. 45, pp. 4767–4769, 2007.

[22] T. N. Murakami, S. Ito, Q. Wang et al., "Highly efficient dye-sensitized solar cells based on carbon black counter electrodes," *Journal of the Electrochemical Society*, vol. 153, no. 12, pp. A2255–A2261, 2006.

[23] M. Yanagida, N. Onozawa-Komatsuzaki, M. Kurashige, K. Sayama, and H. Sugihara, "Optimization of tandem-structured dye-sensitized solar cell," *Solar Energy Materials and Solar Cells*, vol. 94, no. 2, pp. 297–302, 2010.

[24] P. Wang, C. Klein, R. Humphry-Baker, S. M. Zakeeruddin, and M. Grätzel, "A high molar extinction coefficient sensitizer for stable dye-sensitized solar cells," *Journal of the American Chemical Society*, vol. 127, no. 3, pp. 808–809, 2005.

[25] D. Kuang, P. Wang, S. Ito, S. M. Zakeeruddin, and M. Grätzel, "Stable mesoscopic dye-sensitized solar cells based on tetracyanoborate ionic liquid electrolyte," *Journal of the American Chemical Society*, vol. 128, no. 24, pp. 7732–7733, 2006.

[26] N. G. Park, J. van de Lagemaat, and A. J. Frank, "Comparison of dye-sensitized rutile- and anatase-based TiO_2 solar cells," *The Journal of Physical Chemistry B*, vol. 104, no. 38, pp. 8989–8994, 2000.

[27] H. Tsubomura, M. Matsumura, Y. Nomura, and T. Amamiya, "Dye sensitised Zinc oxide: aqueous electrolyte: platinum photocell," *Nature*, vol. 261, no. 5559, pp. 402–403, 1976.

[28] Z. S. Wang, H. Kawauchi, T. Kashima, and H. Arakawa, "Significant influence of TiO_2 photoelectrode morphology on the energy conversion efficiency of N719 dye-sensitized solar cell," *Coordination Chemistry Reviews*, vol. 248, no. 13-14, pp. 1381–1389, 2004.

[29] J. H. Yoon, S. R. Jang, R. Vittal, J. Lee, and K. J. Kim, "TiO_2 nanorods as additive to TiO_2 film for improvement in the performance of dye-sensitized solar cells," *Journal of Photochemistry and Photobiology A*, vol. 180, no. 1-2, pp. 184–188, 2006.

[30] B. Tan and Y. Wu, "Dye-sensitized solar cells based on anatase TiO_2 nanoparticle/nanowire composites," *The Journal of Physical Chemistry B*, vol. 110, no. 32, pp. 15932–15938, 2006.

[31] J. Krč, M. Zeman, F. Smole, and M. Topič, "Optical modeling of a-Si:H solar cells deposited on textured glass/SnO_2 substrates," *Journal of Applied Physics*, vol. 92, no. 2, p. 749, 2002.

[32] M. K. Nazeeruddin, F. De Angelis, S. Fantacci et al., "Combined experimental and DFT-TDDFT computational study of photoelectrochemical cell ruthenium sensitizers," *Journal of the American Chemical Society*, vol. 127, no. 48, pp. 16835–16847, 2005.

[33] S. Ito, N. L. C. Ha, G. Rothenberger et al., "High-efficiency (7.2%) flexible dye-sensitized solar cells with Ti-metal substrate for nanocrystalline-TiO_2 photoanode," *Chemical Communications*, no. 38, pp. 4004–4006, 2006.

[34] M. Grätzel, "Perspectives for dye-sensitized nanocrystalline solar cells," *Progress in Photovoltaics: Research and Applications*, vol. 8, no. 1, pp. 171–185, 2000.

[35] N. Vlachopoulos, P. Liska, J. Augustynski, and M. Grätzel, "Very efficient visible light energy harvesting and conversion by spectral sensitization of high surface area polycrystalline titanium dioxide films," *Journal of the American Chemical Society*, vol. 110, no. 4, pp. 1216–1220, 1988.

[36] H. W. Lin, S. Y. Ku, H. C. Su et al., "Highly efficient visible-blind organic ultraviolet photodetectors," *Advanced Materials*, vol. 17, no. 20, pp. 2489–2493, 2005.

[37] C. J. Yang, T. Y. Cho, C. L. Lin, and C. C. Wu, "Energy-recycling high-contrast organic light-emitting devices," *Journal of the Society for Information Display*, vol. 16, no. 6, pp. 691–694, 2008.

[38] C. J. Lin, W. Y. Yu, and S. H. Chien, "Effect of anodic TiO_2 powder as additive on electron transport properties in nanocrystalline TiO_2 dye-sensitized solar cells," *Applied Physics Letters*, vol. 91, no. 23, Article ID 233120, 2007.

[39] M. Adachi, M. Sakamoto, J. Jiu, Y. Ogata, and S. Isoda, "Determination of parameters of electron transport in dye-sensitized solar cells using electrochemical impedance spectroscopy," *The Journal of Physical Chemistry B*, vol. 110, no. 28, pp. 13872–13880, 2006.

[40] C. C. Chen, B. C. Huang, M. S. Lin et al., "Impedance spectroscopy and equivalent circuits of conductively doped organic hole-transport materials," *Organic Electronics*, vol. 11, no. 12, pp. 1901–1908, 2010.

[41] L. Y. Lin, C. H. Tsai, K. T. Wong et al., "Organic dyes containing coplanar diphenyl-substituted dithienosilole core for efficient dye-sensitized solar cells," *Journal of Organic Chemistry*, vol. 75, no. 14, pp. 4778–4785, 2010.

[42] M. Miyashita, K. Sunahara, T. Nishikawa et al., "Interfacial electron-transfer kinetics in metal-free organic dye-sensitized solar cells: combined effects of molecular structure of dyes and electrolytes," *Journal of the American Chemical Society*, vol. 130, no. 52, pp. 17874–17881, 2008.

[43] L. Y. Lin, C. H. Tsai, K. T. Wong et al., "Efficient organic DSSC sensitizers bearing an electron-deficient pyrimidine as an effective π-spacer," *Journal of Materials Chemistry*, vol. 21, no. 16, pp. 5950–5958, 2011.

[44] J. Bisquert, G. Garcia-Belmonte, F. Fabregat-Santiago, N. S. Ferriols, P. Bogdanoff, and E. C. Pereira, "Doubling Exponent Models for the Analysis of Porous Film Electrodes by Impedance. Relaxation of TiO_2 Nanoporous in Aqueous Solution," *The Journal of Physical Chemistry B*, vol. 104, no. 10, pp. 2287–2298, 2000.

[45] F. Fabregat-Santiago, J. Bisquert, E. Palomares et al., "Correlation between photovoltaic performance and impedance spectroscopy of dye-sensitized solar cells based on ionic liquids," *The Journal of Physical Chemistry C*, vol. 111, no. 17, pp. 6550–6560, 2007.

[46] Q. Wang, J. E. Moser, and M. Grätzel, "Electrochemical impedance spectroscopic analysis of dye-sensitized solar cells," *The Journal of Physical Chemistry B*, vol. 109, no. 31, pp. 14945–14953, 2005.

[47] A. Hauch and A. Georg, "Diffusion in the electrolyte and charge-transfer reaction at the platinum electrode in dye-sensitized solar cells," *Electrochimica Acta*, vol. 46, no. 22, pp. 3457–3466, 2001.

[48] J. R. Macdonald, "Impedance spectroscopy," *Annals of Biomedical Engineering*, vol. 20, no. 3, pp. 289–305, 1992.

[49] A. Georg, W. Graf, R. Neumann, and V. Wittwer, "Mechanism of the gasochromic coloration of porous WO3 films," *Solid State Ionics*, vol. 127, no. 3, pp. 319–328, 2000.

[50] J. D. Roy-Mayhew, D. J. Bozym, C. Punckt, and I. A. Aksay, "Functionalized graphene as a catalytic counter electrode in dye-sensitized solar cells," *ACS Nano*, vol. 4, no. 10, pp. 6203–6211, 2010.

[51] S. Kim, D. Kim, H. Choi et al., "Enhanced photovoltaic performance and long-term stability of quasi-solid-state dye-sensitized solar cells via molecular engineering," *Chemical Communications*, no. 40, pp. 4951–4953, 2008.

[52] N. Kopidakis, N. R. Neale, K. Zhu, J. van de Lagemaat, and A. J. Frank, "Spatial location of transport-limiting traps in TiO_2 nanoparticle films in dye-sensitized solar cells," *Applied Physics Letters*, vol. 87, no. 20, Article ID 202106, 3 pages, 2005.